

# Interferometric $^{12}\text{CO}(\text{J} = 2 - 1)$ image of the Nuclear Region of Seyfert 1 Galaxy NGC 1097

Pei-Ying Hsieh<sup>1,2</sup>, Satoki Matsushita<sup>2</sup>, Jeremy Lim<sup>2</sup>, Kotaro Kohno<sup>3</sup>, Satoko Sawada-Satoh<sup>2,4</sup>  
pyhsieh@asiaa.sinica.edu.tw

<sup>1</sup> *Institute of Astrophysics, National Taiwan University, No.1 Sec. 4 Roosevelt Road, Taipei 10617, Taiwan, R.O.C.*

<sup>2</sup> *Academia Sinica Institute of Astronomy and Astrophysics, P.O. Box 23-141, Taipei 10617, Taiwan, R.O.C.*

<sup>3</sup> *Institute of Astronomy, The University of Tokyo, 2-21-1 Osawa, Mitaka, Tokyo 181-0015, Japan*

<sup>4</sup> *Department of Physics, Faculty of Science, Yamaguchi University, 1677-1 Yoshida, Yamaguchi-City, Yamaguchi 752-8512 JAPAN*

## ABSTRACT

We have mapped the central region of the Seyfert 1 galaxy NGC 1097 in  $^{12}\text{CO}(\text{J} = 2 - 1)$  with the Submillimeter Array (SMA). The  $^{12}\text{CO}(\text{J} = 2 - 1)$  map shows a central concentration and a surrounding ring, which coincide respectively with the Seyfert nucleus and a starburst ring. The line intensity peaks at the nucleus, whereas in a previously published  $^{12}\text{CO}(\text{J} = 1 - 0)$  map the intensity peaks at the starburst ring. The molecular ring has an azimuthally averaged  $^{12}\text{CO}(\text{J} = 2 - 1)/(\text{J} = 1 - 0)$  intensity ratio ( $R_{21}$ ) of about unity, which is similar to those in nearby active star forming galaxies, suggesting that most of the molecular mass in the ring is involved in fueling the starburst. The molecular-gas-to-dynamical mass ratio in the starburst ring shows a somewhat lower value than that found in nearby star forming galaxies, suggesting that the high  $R_{21}$  of unity may be caused by additional effects, such as shocks induced by gas infall along the bar. The molecular gas can last for only about  $1.2 \times 10^8$  years without further replenishment assuming a constant star formation rate and a perfect conversion of gas to stars. The velocity map shows that the central molecular gas is rotating with the molecular ring in the same direction, while its velocity gradient is much steeper than that of the ring. This velocity gradient of the central gas is similar to what is usually observed in some Seyfert 2 galaxies. To

view the active nucleus directly in the optical, the central molecular gas structure can either be a low-inclined disk or torus but not too low to be less massive than the mass of the host galaxy itself, be a highly-inclined thin disk or clumpy and thick torus, or be an inner part of the galactic disk. The  $R_{21}$  value of  $\sim 1.9$  of the central molecular gas component, which is significantly higher than the value found at the molecular gas ring, indicates that the activity of the Seyfert nucleus may have a significant influence on the conditions of the molecular gas in the central component.

*Subject headings:* galaxies: individual (NGC 1097), galaxies: active, galaxies: Seyfert, galaxies: nuclei, galaxies: ISM

## 1. INTRODUCTION

NGC 1097 (SB(s)b; de Vaucouleurs et al. 1991) is a nearby, inclined ( $46^\circ$ ; Ondrechen, van der Hulst, & 1989), barred spiral galaxy at a distance of  $D = 14.5$  Mpc ( $1'' = 70$  pc; Tully 1988). It hosts a Seyfert 1 nucleus, which is surrounded by a circumnuclear starburst ring with a radius of  $10''$  ( $0.7$  kpc). NGC 1097 was originally identified as a LINER (Keel 1983), but over the past two decades has shown Seyfert 1 activity as evidenced by the presence of broad double-peaked Balmer emission lines ( $\text{FWHM} \approx 7500 \text{ km s}^{-1}$ ; Storchi-Bergmann, Baldwin, & Wilson 1993). The starburst ring is rich in molecular gas ( $1.3 \times 10^9 M_\odot$ ; Gerin et al. 1988), and exhibits a high star formation rate of  $5 M_\odot \text{ yr}^{-1}$  as estimated from its extinction-corrected  $\text{H}\alpha$  luminosity (Hummel, van der Hulst, & Keel 1987). A network of dusty spiral features connects the starburst ring with the nucleus (Barth et al. 1995; Prieto, Maciejewski, & Reunanen 2005). Optical spectroscopic imaging observations show evidence for radial streaming motions associated with the spiral structures leading to the unresolved nucleus (Fathi et al. 2006).

Kohno et al. (2003) have previously mapped the central  $\sim 1'$  of NGC 1097 in  $^{12}\text{CO}(J = 1 - 0)$  and  $\text{HCN}(J = 1 - 0)$  with the Nobeyama Millimeter Array (NMA). Their  $^{12}\text{CO}(J = 1 - 0)$  map shows a ring-like structure consisting of several bright knots located at the starburst ring, and this molecular gas ring structure is similar to that revealed by the single dish  $^{12}\text{CO}(J = 1 - 0)$  observations (Gerin et al. 1988). The interferometric  $^{12}\text{CO}(J = 1 - 0)$  map also revealed a relatively weak central concentration coincident with the nucleus. Their  $\text{HCN}(J = 1 - 0)$  map shows similar knots in the starburst ring, but in contrast to their  $^{12}\text{CO}(J = 1 - 0)$  map a relatively bright central concentration of the HCN emission coincides with the nucleus. This implies that the molecular gas associated with the nucleus is relatively dense ( $n_{\text{H}_2} \geq 10^4 \text{ cm}^{-2}$ ). Similar dense central gas concentrations have been reported in NGC 1068 (Jackson et al. 1993), M51 (Kohno et al. 1996), and NGC 6951 (Krips et al. 2007), all

of which are type 2 Seyferts. In all these cases, the dense central gas concentrations have been attributed to a highly inclined circumnuclear molecular torus invoked by AGN unification models (e.g., Antonucci 1993) to obscure the central engine from direct view in the optical. This is the first time, however, that such a dense central gas concentration has been seen in a Seyfert 1 galaxy, warranting observations at higher angular resolutions to determine whether it is a good candidate for the hypothesized circumnuclear molecular torus.

In this paper, we study the central region of NGC 1097 in  $^{12}\text{CO}(J = 2 - 1)$  using the Submillimeter Array (SMA; Ho et al. 2004). While the previous  $\text{HCN}(J = 1 - 0)$  and  $^{12}\text{CO}(J = 1 - 0)$  interferometric observations are suitable for tracing density variations in the molecular gas, they are not suitable for studying variations in the gas temperature. If the  $^{12}\text{CO}(J = 1 - 0)$  line is optically thin, the intensity ratio between the  $^{12}\text{CO}(J = 1 - 0)$  line and the higher- $J$  lines provides constraints on the gas temperature (and density) (e.g., Matsushita et al. 2004). In addition, we observe the  $^{12}\text{CO}(J = 2 - 1)$  line at a factor of 2–3 higher angular resolution than the previous observations in  $^{12}\text{CO}(J = 1 - 0)$  and  $\text{HCN}(J = 1 - 0)$ , allowing us to examine for the first time the spatial-kinematic structure of the central gas concentration.

## 2. OBSERVATIONS AND DATA REDUCTION

We observed the central region of NGC 1097 in the  $^{12}\text{CO}(J = 2 - 1)$  line (rest frequency of 230.538 GHz) with the SMA, which has a primary beam of  $52''$  (3.6 kpc) at this frequency. The receivers were turned to observe the  $^{12}\text{CO}(J = 2 - 1)$  line at the upper side band. The observations were performed on 2004 July 23 and October 1 with eight 6-m antennas in the compact configuration. The 225 GHz zenith opacity of the two observations are  $\sim 0.15$  and  $\sim 0.3$ , and the  $T_{\text{sys,DSB}}$  are  $\sim 200$  K and  $\sim 350$  K respectively. We placed the phase center at  $\alpha_{2000} = 02^{\text{h}}46^{\text{m}}18^{\text{s}}.96$  and  $\delta_{2000} = -30^{\circ}16'28''.897$ , which corresponds to the position of the AGN defined by the intensity peak of the 6-cm continuum emission (Hummel et al. 1987). The SMA correlator has a total bandwidth of 2 GHz, and was configured to provide frequency resolution of 0.8125 MHz ( $\sim 1 \text{ km s}^{-1}$ ) and 3.25 MHz ( $4.2 \text{ km s}^{-1}$ ) for the July 23 and October 1 observations respectively. We observed Uranus for bandpass and absolute flux calibrations. We used J0132–169 and J0423–013 for complex gain calibrations. J0132–169 is weaker but closer to the source ( $21^{\circ}.5$  away), and was used for phase calibration only; J0423–013 is stronger but further from the source ( $37^{\circ}$  away), and used for amplitude calibration. The absolute flux accuracy and the positional accuracy have been estimated as  $\sim 15\%$  and  $0''.1$ , respectively, in these observations.

The observation on July 23 was binned to the same velocity resolutions as that on

October 1 (3.25 MHz), and then combined with each other. The data were calibrated with the Owens Valley Radio Observatory software package MIR, which was modified for the SMA. The images were CLEANed using the NRAO software package AIPS, and with natural weighting have an angular resolution of  $4''.1 \times 3''.1$  ( $290 \text{ pc} \times 220 \text{ pc}$ ) at a position angle (P.A.) of  $168^\circ$ . The rms noise level of the individual channel maps is  $75 \text{ mJy beam}^{-1}$ . We used the “MOMNT” task in AIPS to make the integrated intensity and the intensity-weighted mean-velocity maps. The line free channels were binned to create a continuum map with a rms noise level of  $4.4 \text{ mJy beam}^{-1}$ ; no significant emission was detected in this map.

### 3. RESULTS

We detected the  $^{12}\text{CO}(J = 2 - 1)$  line spanning a total line width of  $\sim 570 \text{ km s}^{-1}$  at the  $3\sigma$  detection threshold in the channel maps. The line width is comparable to that measured in the single-dish observation (Petitpas & Wilson 2003) of  $\sim 550 \text{ km s}^{-1}$  using the JCMT, which has a primary beam of  $21''$ , although the integrated line intensity in our map is only  $60 \pm 13\%$  of that measured in this single-dish observation (see Sect. 3.3) including uncertainties of the flux in both observations.

#### 3.1. Spatial Distribution

We show the  $^{12}\text{CO}(J = 2 - 1)$  integrated intensity map in Figure 1(a). A relatively strong molecular concentration (hereafter, central component) is detected at the very center in a region of a diameter of  $350 \text{ pc}$  ( $5''$ ), surrounded by a weaker molecular ring of a diameter of  $1.4 \text{ kpc}$  ( $20''$ ). The centroid of the central molecular gas component is shifted by  $\sim 0''.7$  from that of the radio continuum core at  $6 \text{ cm}$ , which presumably marks the location of the AGN (Hummel et al. 1987). We shall return to this positional difference in Section 3.2.

The molecular ring coincides with the starburst ring, consistent with the previous  $^{12}\text{CO}(J = 1 - 0)$  maps (Gerin et al. 1988; Kohno et al. 2003). Unlike the tightly-wound spiral structure seen in optical maps (e.g., Rickard 1975; Barth et al. 1995), the molecular ring traces a complete circle as seen in the  $J - K_S$  color map of Prieto et al. (2005). The molecular ring is composed of several knots that closely resembles the  $1.5 \text{ GHz}$  continuum map of Hummel et al. (1987). In addition, we detected weak molecular emission extending from the NE and SW of the molecular ring, coinciding with dust lanes along the large stellar bar (indicated by the two straight lines in Fig. 1a).

In Figure 1(b), we show the  $^{12}\text{CO}(J = 1 - 0)$  map made by Kohno et al. (2003) with the NMA. As can be seen, the molecular ring is more clearly discernible and also more clearly separated in our  $^{12}\text{CO}(J = 2 - 1)$  map than in the  $^{12}\text{CO}(J = 1 - 0)$  map. The intensity peak in the  $^{12}\text{CO}(J = 2 - 1)$  map is located at the nucleus, whereas that in the  $^{12}\text{CO}(J = 1 - 0)$  map is located at the NE part of the ring. The SW side of the ring is brighter than the NE side in the  $^{12}\text{CO}(J = 2 - 1)$  map, but the reverse is true in the  $^{12}\text{CO}(J = 1 - 0)$  map. Both of the molecular gas peaks at the NE and SW sides of the ring are located at the regions where the dust lanes connect with the ring, and these molecular gas peaks are often seen in barred spiral galaxies, which are known as the twin-peak morphology (e.g., Kenney et al. 1992).

### 3.2. Kinematics

In Figure 2(a), we show the intensity-weighted  $^{12}\text{CO}(J = 2 - 1)$  mean-velocity map. Both the central component and molecular ring show an overall velocity gradient in the NE to SE direction along a P.A. of  $135^\circ$ , that is similar to the major kinematic axis of the large-scale galactic disk (Ondrechen et al. 1989). The emission is blueshifted on the northwestern side of center, and redshifted on the southeastern side of center with respect to the systemic velocity of  $1254 \text{ km s}^{-1}$  for NGC 1097 (Kohno et al. 2003). The gas motion in the molecular ring appears to be dominated by circular motion (i.e., isovelocity contours perpendicular to major axis), whereas in the  $^{12}\text{CO}(J = 1 - 0)$  velocity map of Kohno et al. (2003) the isovelocity contours have a symmetric S-shape with the end of the S-shape nearly parallel to the dust lanes along the large stellar bar. This non-circular motion is not as prominent in our  $^{12}\text{CO}(J = 2 - 1)$  map perhaps because the aforementioned dust lanes are not as strongly detected in  $^{12}\text{CO}(J = 2 - 1)$ , along with the fact that they are closer to the edge of our primary beam than in the  $^{12}\text{CO}(J = 1 - 0)$  observations of Kohno et al. (2003).

A position-velocity diagram (hereafter p-v diagram) of the  $^{12}\text{CO}(J = 2 - 1)$  emission along its major kinematical axis (P.A. =  $135^\circ$ ) is shown in Figure 2(b). Positive and negative velocities correspond to redshifted and blueshifted velocities, respectively, relative to the systemic velocity. The rapidly rising part of the rotation curve corresponds to the central component, and the flat part to the molecular ring. The rotation curve is symmetric on both sides of the center, rising steeply to  $\pm 235 \text{ km s}^{-1}$  at  $\pm 2''.5$  ( $\pm 175 \text{ pc}$ ) and flattening outside  $\pm 2''.5$ . This indicates that the size of the central component is about  $350 \text{ pc}$  in diameter. As can be seen in Figure 2(b), the emission from the central component is stronger on the redshifted southeastern part, causing the centroid of the emission to be shifted by  $0''.7$  towards the southeast as mention in Section 3.1 (and shown in Fig. 1a). The velocity gradient of the

central component is  $1.31 \pm 0.14 \text{ km s}^{-1} \text{ pc}^{-1}$  (Fig. 1b), which is similar with that derived in the optical from ionized gas ( $\sim 1.1 \text{ km s}^{-1} \text{ pc}^{-1}$ ; Storchi-Bergmann, Wilson, & Baldwin 1996).

### 3.3. $^{12}\text{CO}(J = 2 - 1)/(J = 1 - 0)$ Line Ratios

Our  $^{12}\text{CO}(J = 2 - 1)$  map detected about 60% of the flux measured with the JCMT (Petitpas & Wilson 2003). The shortest projected baseline in our SMA observations is  $4.8 \text{ k}\lambda$  ( $\sim 6 \text{ m}$ ), and so the largest structure we can detect is  $\sim 52''$ , comparable in size to the SMA primary beam. We therefore assume that the molecular gas resolved out in our map is uniformly distributed in space and in velocity over the entire line width, and have corrected for  $\sim 40\%$  of the missing flux. We applied a primary beam correction to both the  $^{12}\text{CO}(J = 2 - 1)$  and  $^{12}\text{CO}(J = 1 - 0)$  maps, and convolved the derived moment maps to the same angular resolution of  $6''.5 \times 3''.5$  with P.A. of  $0^\circ$ . These moment maps were then used to derive the  $^{12}\text{CO}(J = 2 - 1)/^{12}\text{CO}(J = 1 - 0)$  line ratios. Note that we also calculated the line ratios with  $uv$ -matched data, and the ratios are consistent with the missing flux corrected line ratios within errors. To derive the molecular gas column densities and masses, we need to use the missing flux corrected data (see Sect. 3.4). To make consistency within this paper, we use the missing flux corrected data for the following calculations.

In Figure 3, we show the azimuthally averaged radial intensity distributions of the  $^{12}\text{CO}(J = 2 - 1)$  (dashed line) and  $^{12}\text{CO}(J = 1 - 0)$  (dotted line) lines, and the azimuthally averaged  $^{12}\text{CO}(J = 2 - 1)/^{12}\text{CO}(J = 1 - 0)$  line intensity ratio ( $R_{21}$ )(solid line). The radial intensity profile in both  $^{12}\text{CO}(J = 2 - 1)$  and  $^{12}\text{CO}(J = 1 - 0)$  peak at the center, corresponding to the central component, and exhibit a secondary peak at a radius of  $10''$ , corresponding to the molecular ring. The line ratio  $R_{21}$  exhibits a similar behavior, peaking at the central component and exhibiting a secondary peak at the molecular ring. At the nucleus,  $R_{21}$  is derived as  $1.9 \pm 0.2$  at a beam size of  $6''.5 \times 3''.5$ , which corresponds to the approximate angular extent of the central component along its major kinematic axis. In the molecular ring, the azimuthally averaged value between radii of  $8''$  and  $12''$  is  $R_{21} = 1.3 \pm 0.2$ .

The averaged  $R_{21}$  at the molecular ring is similar to or somewhat larger than the global  $R_{21}$  in spiral galaxies of  $\sim 0.7 - 0.9$  (Braine et al. 1993; Lavezzi et al. 1999; Hafok & Stutzki 2003). The  $R_{21}$  at giant molecular clouds (GMCs) in the nearby star forming region Orion (Sakamoto et al. 1994) or GMC-scale  $R_{21}$  in the nearby starburst galaxy M82 (Weiss et al. 2001) also shows similar  $R_{21}$  of about unity. On the other hand, the  $R_{21}$  at the central component is about twice as high as those in the abovementioned sources, and consistent with the ratio reported in the Seyfert 2 galaxy NGC 1068 (Baker & Scoville 1998; Schinnerer et al.

2000). The  $R_{21}$  at the central component is also similar to that found at active star forming regions or at the interfaces of molecular clouds and ionized gas in the nearby barred spiral galaxy IC 342 (Turner, Hurt, & Hudson 1993; Meier, Turner, & Hurt 2000). Galactic objects, such as molecular outflows from young stellar objects (e.g., Richardson et al. 1985; Chandler et al. 1996) or molecular gas around supernova remnants (van Dishoeck, Jansen, & Phillips 1993; Seta et al. 1998) also show  $R_{21} \gtrsim 2$ . Note however that the high value of  $R_{21}$  are not always seen in active galaxies; for instance, interferometric observations of NGC 3227 (Seyfert 1; Schinnerer, Eckart, & Tacconi 2000), NGC 3718 (LINER/Seyfert 1; Krips et al. 2005), and NGC 6574 (Seyfert 2; Lindt-Krieg et al. 2008) show  $R_{21}$  of around unity.

### 3.4. Physical Properties of the Molecular Gas

We derived the column density of the molecular gas in the central component and molecular ring assuming the standard Galactic conversion factor of  $3.0 \times 10^{20} \text{ cm}^{-2} (\text{K km s}^{-1})^{-1}$  between the  $^{12}\text{CO}(J = 1 - 0)$  line intensity and column density of molecular hydrogen gas (Scoville et al. 1987; Solomon et al. 1987). The  $^{12}\text{CO}(J = 2 - 1)$  integrated intensity at the center (beam size of  $3''.1 \times 4''.1$ ) is  $376.7 \pm 7.2 \text{ K km s}^{-1}$ . Assuming the same line ratios derived from a beam size of  $6''.5 \times 3''.5$ , namely,  $R_{21} = 1.9 \pm 0.2$  for the central component, we derive a column density for this component of  $(5.9 \pm 0.6) \times 10^{22} \text{ cm}^{-2}$ , and the molecular hydrogen gas mass of  $(6.5 \pm 0.7) \times 10^7 \text{ M}_{\odot}$ . In the molecular ring, the azimuthally averaged  $^{12}\text{CO}(J = 2 - 1)$  integrated intensity between the radii of  $8''$  and  $12''$  is  $135.7 \pm 7.2 \text{ K km s}^{-1}$ . With  $R_{21} = 1.3 \pm 0.2$ , the azimuthally averaged column density at the molecular ring is therefore  $(3.0 \pm 0.3) \times 10^{22} \text{ cm}^{-2}$ , and the molecular hydrogen gas mass is  $(5.8 \pm 0.6) \times 10^8 \text{ M}_{\odot}$ . Here we compare our estimated molecular gas mass of the ring with that estimated using the single-dish data. We re-calculated the gas mass inside  $20''$  in radius derived by Gerin et al. (1988) using the conversion factor mentioned above, and it is calculated as  $1.1 \times 10^9 \text{ M}_{\odot}$ . We then subtract the gas mass of the center from this gas mass. The gas mass of the center is calculated as  $2.4 \times 10^8 \text{ M}_{\odot}$  using the central position data with a  $T_b$  of  $\sim 32 \text{ K km s}^{-1}$  (Fig. 3 of Gerin et al. (1988)). The gas mass of the ring is therefore calculated as  $\sim 8.6 \times 10^8 \text{ M}_{\odot}$ . This value is somewhat larger than ours, and this may be due to their larger radius of  $20''$ , and therefore their results may be detecting emission outside the ring.

To determine the temperature and density of the molecular gas, we use the LVG method (Goldreich & Kwan 1974). We assume a one zone model, which assumes that both the  $^{12}\text{CO}(J = 2 - 1)$  and  $^{12}\text{CO}(J = 1 - 0)$  emissions originate from the same region. The collision rates for CO are taken from Flower & Launay (1985) for the temperature regime  $T = 10 - 250 \text{ K}$ , and McKee et al. (1982) for  $T = 500 - 1000 \text{ K}$ . We first assume a stan-

standard  $Z(^{12}\text{CO})/(dv/dr)$  of  $5.0 \times 10^{-5} \text{ (km s}^{-1} \text{ pc}^{-1})^{-1}$ , where  $Z(^{12}\text{CO}) = [^{12}\text{CO}]/[\text{H}_2]$  is the abundance ratio and  $dv/dr$  is the velocity gradient of the molecular gas.

We then compute from the LVG model the line ratio  $R_{21}$  and  $^{12}\text{CO}(J = 1 - 0)$  opacity as a function of molecular hydrogen number density  $n_{\text{H}_2}$  and kinetic temperature  $T_k$  as shown in Figure 4(a). The result for  $R_{21} = 1.9 \pm 0.2$  as inferred for the central component indicates that  $T_k \geq 400 \text{ K}$ , and  $n_{\text{H}_2} \sim 3 \times 10^{4 \pm 1} \text{ cm}^{-3}$ , and  $^{12}\text{CO}(J = 1 - 0)$  opacity below unity. The density estimation is consistent with the detection of  $\text{HCN}(J = 1 - 0)$  line from the central component (Kohno et al. 2003), which indicates the molecular gas density as high as  $n_{\text{H}_2} \approx 10^4 \text{ cm}^{-3}$ . Note that the estimated kinetic temperature is highly dependent on the assumed  $Z(^{12}\text{CO})/(dv/dr)$ , namely highly dependent on the  $[^{12}\text{CO}]/[\text{H}_2]$  relative abundance, on the velocity gradient, or on both. Fixing  $n_{\text{H}_2} = 1 \times 10^4 \text{ cm}^{-3}$ , we plot  $R_{21}$  as a function of  $T_k$  and  $Z(^{12}\text{CO})/(dv/dr)$  in Figure 4(b). As can be seen,  $R_{21}$  increases roughly linearly with  $Z(^{12}\text{CO})/(dv/dr)$ , and around the standard  $Z(^{12}\text{CO})/(dv/dr)$  of  $\approx 10^{-5} \text{ (km s}^{-1} \text{ pc}^{-1})^{-1}$ , we find that a kinetic temperature of at least 100 K is required to reach  $R_{21}$  of  $1.9 \pm 0.2$ . If on the other hand  $Z(^{12}\text{CO})/(dv/dr)$  is an order of magnitude lower than the standard value (i.e., order of  $10^{-6}$ ), the kinetic temperature would be in the range of  $T_k \approx 30 - 250 \text{ K}$ , which is comparable with the temperature range normally found in molecular clouds.

For the molecular ring, which has an average  $R_{21} = 1.3 \pm 0.2$ ,  $T_k \gtrsim 100 \text{ K}$  and  $n_{\text{H}_2} \sim 1 \times 10^{4 \pm 1} \text{ cm}^{-3}$  assuming the standard  $Z(^{12}\text{CO})/(dv/dr)$ . Again, these values are sensitive to the assumed  $Z(^{12}\text{CO})/(dv/dr)$ , and if this value decreases,  $T_k$  and  $n_{\text{H}_2}$  also decrease.

## 4. DISCUSSIONS

### 4.1. Molecular Gas in the Starburst Ring

The average  $R_{21}$  of about unity in the molecular ring suggests that the overall properties of the molecular gas in the starburst ring is optically thick and thermalized. As mentioned in Section 3.3, this value is similar to that of the global  $R_{21}$  of other spiral galaxies or that in the active star forming GMCs. Similarity of the molecular gas ratios between the molecular gas in the ring and the molecular clouds at active star forming regions indicates that the molecular gas in the ring is closely related to the starburst activities occurring in the ring. This is also supported by the high  $\text{HCN}(J = 1 - 0)/^{12}\text{CO}(J = 1 - 0)$  of 0.16 (Kohno et al. 2003). Since stars form from molecular gas, we believe that this molecular gas is actually fueling the starburst activities in the ring. The gas mass content in the starburst ring is, on the other hand, not as high as star forming galaxies, about 8% of the dynamical mass; the dynamical mass within the radius of  $8'' - 12''$  (560 – 840 pc; roughly corresponds to the



width of the molecular ring) can be estimated as  $(6.9 \pm 0.2) \times 10^9 M_\odot$ , using the rotational velocity of  $235 \text{ km s}^{-1}$  (Sect. 3.2) and assuming the inclination of the molecular ring is the same as that of the host galaxy of  $46^\circ$  (Ondrechen et al. 1989). The molecular gas mass in the ring is  $5.8 \times 10^8 M_\odot$  (Sect. 3.4), so that the molecular gas mass to dynamical mass ratio is calculated as  $(8 \pm 1)\%$ . This value is a bit lower than the threshold to have star formation activities at nuclei of  $\sim 10\%$  suggested by Sakamoto et al. (1999). One reason for the discrepancy between high  $R_{21}$  and  $\text{HCN}(J = 1 - 0)/^{12}\text{CO}(J = 1 - 0)$  ratios and low molecular gas mass to dynamical mass ratio may be that Sakamoto et al. (1999) are taking mass ratios within 500 pc in radius, but we are taking the mass ratio in a certain range of radius. Another possibilities is that the gas in the staburst ring is highly affected by shock induced by the gas infall along the bar, so that the high intensity ratios may not tracing the star formation activities, but tracing shocked gas.

The upper limit of the mass of newly formed (1.5 Gyr old) stars in the star-forming ring is  $\sim 10^9 M_\odot$  (Quillen et al. 1995), which is roughly comparable to or somewhat larger than the mass of molecular gas ( $5.8 \times 10^8 M_\odot$ ). This implies that a large fraction of the molecular gas has already turned into stars within a timescale of 1.5 Gyr. We can estimate the molecular gas consumption timescale with considering the star formation rate (SFR) and the molecular gas mass of the ring. The SFR in the molecular ring is about  $5 M_\odot \text{ yr}^{-1}$  (Hummel et al. 1987). Without further replenishment, the molecular gas in the ring can last for only about  $(1.2 \pm 0.1) \times 10^8$  years assuming a constant SFR and a perfect conversion of gas to stars. This value is roughly an order of magnitude lower than the value derived by Gerin et al. (1988), which is due to their somewhat larger molecular gas mass, inclusion of atomic hydrogen gas mass assuming it has the same amount as the molecular gas mass, and using lower SFR of  $\sim 2 M_\odot \text{ yr}^{-1}$ . In addition to the gas consumption by star formation, the amount of molecular gas in the ring also decreases by the infall toward the nucleus. As mentioned in Section 1, the gas infalling motion has been observed from the ring to the nucleus. The value for the mass infall rate is not known, but this effect obviously decreases the lifetime of the molecular ring. On the other hand, gas replenishment by the infall along the large scale bar from the outer part of the galaxy to the molecular ring increases the lifetime. The value for the mass infall rate is again not known, so the lifetime of the molecular ring is decided by the balance between these effects.

## 4.2. Nature of the Nuclear Component

Our  $^{12}\text{CO}(J = 2 - 1)$  results show that the molecular gas located at the center is spatially coincident with the AGN, which is consistent with the previous interferometric maps of the

$^{12}\text{CO}(J = 1 - 0)$  and  $\text{HCN}(J = 1 - 0)$  lines (Kohno et al. 2003). In addition, the central component is kinematically symmetric at the center with steep velocity gradient, suggesting that the molecular gas is rotating around the AGN. Here we discuss the relation between the central component and the AGN activities based on the line ratios of the central component and its physical conditions, which were derived using the LVG analysis results presented in the previous section.

The  $^{12}\text{CO}(J = 2 - 1)$  map peaks at the nucleus, different from the  $^{12}\text{CO}(J = 1 - 0)$  map, and the  $R_{21}$  shows  $1.9 \pm 0.2$ . This value is significantly higher value than the global  $R_{21}$  of spiral galaxies or  $R_{21}$  in star forming GMCs in Orion or M82, but similar to the  $R_{21}$  of molecular gas at jets, at supernova remnants, or at the surface between molecular gas and ionized gas (Sect. 3.3). These results suggest that the high  $R_{21}$  in molecular gas can be related to irradiation of UV photons from star forming regions, shock caused by interaction between molecular gas and outflowing or expanding materials, but not to the global galactic characteristics or activities. Hence similar activities can be the cause of high  $R_{21}$  in the central region of NGC 1097. However, other activities that cannot be seen in star forming galaxies or in our Galaxy can also be the cause of high  $R_{21}$ , such as strong X-ray radiation from the Seyfert 1 nucleus (e.g., Lepp & Dalgarno 1996; Kohno et al. 2001; Usero et al. 2004; Kohno 2005; Meijerink, Spaans, & Israel 2007).

From LVG analysis, high temperature ( $\gtrsim 400$  K) and high density ( $\sim 3 \times 10^{4\pm1} \text{ cm}^{-3}$ ) conditions are derived for the central component, assuming a standard  $Z(^{12}\text{CO})/(dv/dr)$ . As mentioned in Section 3.4, the density is consistent with the centrally peaked  $\text{HCN}(1 - 0)$  map (Kohno et al. 2003). Furthermore, these conditions are supported by results from infrared observations: Strong molecular hydrogen line,  $\text{H}_2 1 - 0 \text{ S}(1)$ , is detected toward the nucleus without any detection of  $\text{Br}\gamma$  line, and the  $JHK$  images show red colors toward the nucleus, suggesting that the presence of hot dust coexisting with the dense molecular gas (Kotilainen et al. 2000). Such high density and high temperature conditions for molecular gas around Seyfert nuclei are also derived in other galaxies, such as the Seyfert 2 nucleus of M51 (Matsushita et al. 1998, 2004) or NGC 1068 (Rotaciuc et al. 1991; Tacconi et al. 1994), but not for the molecular gas in non-active galaxies such as IC 342 or our Galaxy (Matsushita et al. 1998). These physical values are, however, sensitive to  $Z(^{12}\text{CO})/(dv/dr)$ , namely to the  $^{12}\text{CO}$  abundances, to the velocity gradient, or to both. As shown in Section 3.4, lower  $Z(^{12}\text{CO})/(dv/dr)$  makes the derived temperature lower. This is because the opacity is linearly related to  $Z(^{12}\text{CO})/(dv/dr)$ , and it will decrease if  $Z(^{12}\text{CO})/(dv/dr)$  decreases. Under low  $Z(^{12}\text{CO})/(dv/dr)$  conditions, if the temperature rises, the  $^{12}\text{CO}(J = 1 - 0)$  line can easily be optically thin, and easier to have high  $R_{21}$  at lower temperature than the normal  $Z(^{12}\text{CO})/(dv/dr)$  condition. In either case, the molecular gas around Seyfert nuclei seems to have different properties from other normal environment, which seems to be largely

related to the Seyfert activities. Combined with the spatial and kinematical information, we suggest that the central component is kinematically and physically related to the Seyfert nucleus.

### 4.3. Is the Circumnuclear Gas the Hypothetical Circumnuclear Torus?

Given that the central component is closely related to the AGN, is this then the circumnuclear molecular torus predicted by AGN unified models? Since NGC 1097 hosts a Seyfert 1 AGN, we expect that the rotating circumnuclear gas is in a nearly face-on configuration to provide an essentially unobscured view to the broad-line region (BLR), if we apply the general unified model for AGNs (e.g., Antonucci 1993). Kinematics of the central component we observed are, however, similar to what is usually observed in other Seyfert 2 galaxies, such as NGC 1068 (Jackson et al. 1993; Schinnerer et al. 2000) or M51 (Kohno et al. 1996; Scoville et al. 1998); the central component shows steep velocity gradient that can be explained by edge-on disk or torus rotating around the Seyfert nucleus. In addition, we derived a molecular hydrogen column density ( $N_{\text{H}_2}$ ) toward the nucleus of  $(5.9 \pm 0.6) \times 10^{22} \text{ cm}^{-2}$  (Sect. 3.4), or  $1.2 \times 10^{23} \text{ cm}^{-2}$  in atomic hydrogen column density ( $N_{\text{H}}$ ), which is about two orders of magnitudes larger than  $N_{\text{H}}$  derived from X-ray spectra of  $1.3 \times 10^{21} \text{ cm}^{-2}$  (Iyomoto et al. 1996; Terashima et al. 2002).

From these “inconsistent” results between our molecular gas observations and other observations at different wavelengths/frequencies, the structure of the central component can have two basic configurations; one is a nearly face-on disk-, ring-, or torus-like structure with a very fast rotation velocity, and another is a nearly edge-on disk-, ring-, or torus-like structure with a thin or clumpy structure. Due to our large synthesized beam size, we could not distinguish these two possibilities observationally, and also could not evaluate the thickness of the structure. Here we discuss the advantages and disadvantages of both possibilities.

The former molecular gas configuration has a nearly face-on structure, so the direct view to the BLR is secured. But since the observed rotational velocity width has  $470 \text{ km s}^{-1}$ , the inclination corrected rotational velocity width for this configuration has to be  $470 \sin(i)$ , where  $i$  is the inclination ( $0^\circ$  corresponds to a face-on configuration). The nearly face-on configuration therefore leads to a high rotational velocity (e.g.,  $940 \text{ km s}^{-1}$  even for the inclination angle of  $30^\circ$ ). Note that this rotation is rigid rotation, and it is rare to see rigid rotation velocity of  $> 500 \text{ km s}^{-1}$  in other galaxies (e.g., Rubin, Thonnard, & Ford 1980; Rubin et al. 1982; Sofue et al. 1999). In addition, assuming the inclination angles as  $30^\circ$ ,  $10^\circ$ , and  $5^\circ$ , the dynamical mass within the central gas, namely within the radius of  $2''.5$  (175 pc),

can be estimated to be  $8.8 \times 10^9 M_\odot$ ,  $7.3 \times 10^{10} M_\odot$ , and  $2.9 \times 10^{11} M_\odot$ , respectively. The total dynamical mass of NGC 1097 within a radius of 7.5 (31.5 kpc) estimated from the large-scale atomic hydrogen observations is  $(5.0 \pm 0.8) \times 10^{11} M_\odot$  (Higdon & Wallin 2003). A disk with the inclination angle of  $5^\circ$  is impossible, since the dynamical mass of the central gas is almost the same with the mass of the whole galaxies. A disk with the inclination angle of  $10^\circ$  is still too large, since more than one tenth of the total mass is concentrated within a thousandth of radius. A disk with the inclination angle of  $30^\circ$  can be possible. We therefore think that this face-on configuration can be possible, only if the inclination angle is  $\sim 30^\circ$  or larger.

The latter molecular gas configuration has an edge-on structure, so the structure should have thin disk- or ring-like structure, or it can be torus-like structure but has to have a clumpy internal structure to expose the BLR at the center. Such clumpy structure is suggested theoretically (Wada & Norman 2002), and with their model, the column density of  $\sim 10^{21} \text{ cm}^{-2}$  is possible even with the inclination angle of  $\sim 60^\circ$ . Under this model, the difference of the column density derived from our CO data and from the X-ray data can be explained; the spatial resolution of our observation is about 250 pc, which smears all the internal clumpy structures, and therefore the derived column density will be the average value and higher than that derived from X-ray observations, which only trace very narrow column densities due to the very small size scale of the X-ray emitting region ( $< 1 \text{ pc}$ ). Under these nearly edge-on configurations, the rotational velocity is in the typical values for other galaxies ( $< 500 \text{ km s}^{-1}$ ), and therefore we do not need to invoke any special conditions.

Of course, there is another possibility that the central component is nothing related to the hypothetical torus, namely the central component we observed is just a part of the galactic disk gas. This is supported by the similar trend and the smooth connection of the molecular gas kinematics at the nucleus and the ring. Since the infalling motion exists from the ring to the nucleus along the nuclear bar or spiral (Prieto et al. 2005; Fathi et al. 2006), it is natural to pile up the gas around the nucleus with similar kinematics as that of the ring. In this case, gas will rotate around the nucleus with similar inclination as the outer disk or the ring, and it is natural not to cover the line-of-sight toward the AGN, namely the gas configuration will be similar to the Seyfert 1 nucleus. In addition, if the molecular gas piles up at the diameter smaller than our beam size of 200–300 pc, the discrepancy of the column density estimated from our data and the X-ray data can also be explained. Here we briefly estimate the necessary gas infall rate to create the central component with gas infall from the molecular ring. The  $\text{H}_2$  masses of the central component is  $6.5 \times 10^7 M_\odot$ , so that the mass infall rate of  $0.5 M_\odot \text{ yr}^{-1}$  is required to create this component within the molecular ring gas consumption timescale of  $1.2 \times 10^8$  years (Sect. 4.1). Note that the line ratio of the central component is obviously different from that in other regions or other galaxies, and

this can be explained either by the shock caused by the gas inflow along the nuclear bar or nuclear spiral, or by AGN activities, such as irradiation of strong X-ray emission to the central component.

In summary, the central component can be the hypothetical circumnuclear disk or torus with nearly edge-on ( $\gtrsim 60^\circ$ ) clumpy structure, or less likely nearly face-on ( $\gtrsim 30^\circ$ ) disk/torus. The central component can also be nothing related to the hypothetical disk/torus, and possibly created by the gas inflow from the molecular ring. The physical conditions of the central component are different from that of molecular gas in other regions, so that even it is not the hypothetical disk/torus, it should be highly related to the AGN activities or gas inflow toward the nucleus.

## 5. SUMMARY

We successfully imaged the central component and the molecular ring, which is spatially coincident with the AGN and the starburst ring, toward the central region of the Seyfert 1 galaxy NGC 1097 using the SMA in the  $^{12}\text{CO}(J = 2 - 1)$  line. Here are the summary for the nature of the central component we observed:

1. We found that the  $^{12}\text{CO}(J = 2 - 1)$  map shows an intensity peak at the central component, and different from the  $^{12}\text{CO}(J = 1 - 0)$  map, which shows the intensity peak at the molecular ring.
2. The  $^{12}\text{CO}(J = 2 - 1)/^{12}\text{CO}(J = 1 - 0)$  line intensity ratio for the central component is  $1.9 \pm 0.2$ , which is different from the global values in GMCs or in spiral galaxies of about unity or less. From the LVG analysis, we estimated that the central component is warmer ( $T_K \gtrsim 400$  K) and denser ( $n_{\text{H}_2} \sim 3 \times 10^4 \text{ cm}^{-3}$ ) than that of the normal molecular clouds assuming a normal  $Z(^{12}\text{CO})/(dv/dr)$ . These values depend highly on the  $Z(^{12}\text{CO})/(dv/dr)$ , and lower  $Z(^{12}\text{CO})/(dv/dr)$  for about an order of magnitude decreases the temperature and density of about an order of magnitude. The effect of intense star formation and/or AGN activities, such as shocks induced by numerous supernova explosions or strong X-ray radiation from AGN are presumably the causes of the unusual line ratio.
3. Faster rotation feature of the central gas is observed in NGC 1097, which is similar results as observed in other Seyfert 2 galaxies. We interpret this feature as a highly-inclined clumpy disk/torus or thin disk to explain the fast rotation and the difference between the column density derived from CO and X-ray observations. A low-inclined

( $i \sim 30^\circ$ ) thick disk is possible, but lower inclination than this value is less likely since it is rare to see a velocity  $\geq 500 \text{ km s}^{-1}$  in nearby galaxies, and the total mass of central disk turns to be too large compared with the total mass of the galaxy. On the other hand, the central component can also be interpreted as just an inner extension of the galactic disk, possibly created by the gas inflow from the molecular ring.

4. Combining kinematical and spatial information with the physical conditions, we suggest that the central gas is related to the Seyfert activities or gas inflow.

Here are the summary for the nature of the molecular ring we observed:

1. The  $R_{21}$  of the molecular ring is  $1.3 \pm 0.2$ , which shows a similar properties to the star forming GMCs in our Galaxy or nearby starburst galaxies. In addition, since the molecular ring shows a good spatial coincident with the starburst ring, so we expect that the molecular ring is actually fueling the starburst activities. The molecular gas mass content with respect to the dynamical mass, on the other hand, shows somewhat low value, so that high  $R_{21}$  may not be related to star formation activities, but to other activities, such as shock induced by gas infall along the bar. Without further replenishment, it can last for only about  $1.2 \times 10^8$  years, but since there seems to have gas flows from the dust lane along the large-scale bar toward the molecular ring, and from the molecular ring toward the nucleus, this timescale is highly uncertain.

We would like to acknowledge the anonymous referee for the valuable discussions and comments. We also thank for the SMA staff for maintaining the operation of the array. The Submillimeter Array is a joint project between the Smithsonian Astrophysical Observatory and the Academia Sinica Institute of Astronomy and Astrophysics and is funded by the Smithsonian Institution and the Academia Sinica. This work is supported by the National Science Council (NSC) of Taiwan, NSC 96-2112-M-001-0095.

## REFERENCES

- Antonucci, R. 1993, ARA&A, 31, 473
- Barth, A. J., Ho, L. C., Filippenko, A. V., & Sargent, W. L. 1995, AJ, 110, 1009
- Braine, J., Combes, F., Casoli, F., Dupraz, C., Gerin, M., Klein, U., Wielebinski, R., & Brouillet, N. 1993, A&AS, 97, 887
- Baker, A. J. & Scoville, N. Z. 1998, IAUS, 184, 221
- Chandler, C. J., Terebey, S., Barsony, M., Moore, T. J. T., & Gautier, T. N. 1996, ApJ, 471, 308
- de Vaucouleurs, G., de Vaucouleurs, A., Corwin, H. G., Jr., Buta, R. J., Paturel, G., & Fouqué, P. 1991, Third Reference Catalogue of Bright Galaxies (New York: Springer-Verlag)
- Fathi, K., Storchi-Bergmann, T., Riffel, R. A., Winge, C., Axon, D. J., Robinson, A., Capetti, A., & Marconi, A. 2006, ApJ, 641, L25
- Flower, D. R., & Launay, J. M. 1985, MNRAS, 241, 271
- Gerin, M., Nakai, N., & Combes, F. 1988, A&A, 203, 44
- Goldreich, P., & Kwan, J. 1974, ApJ, 189, 441
- Hafok, H., & Stutzki, J. 2003, A&A, 398, 959
- Ho, P. T. P., Moran, J. M., & Lo, F. 2004, ApJ, 616, L1
- Higdon, J. L. & Wallin, J. F. 2003, ApJ, 585, 281
- Hummel, E., van der Hulst, J. M., & Keel, W. C. 1987, A&A, 172, 32
- Iyomoto, N., Makishima, K., Fukazawa, Y., Tashiro, M., Ishisaki, Y., Nakai, N., & Taniguchi, Y. 1996, PASJ, 48, 231
- Jackson, M., Paglione, T. A. D., Ishizuki, S., & Nguyen-Q-Rieu 1993, ApJ, 418, L13
- Keel, W. C. 1983, ApJ, 269, 466
- Kenney, J. D. P., Wilson, C. D., Scoville, N. Z., Devereux, N. A., Young, J. S. 1992, ApJ, 395, 79

- Kohno, K., Kawabe, R., Tosaki T., & Okumura S. K. 1996, *ApJ*, 461, L29
- Kohno, K., Matsushita, S., Vila-Vilaró, B., Okumura, S. K., Shibatsuka, T., Okiura, M., Ishizuki, S., & Kawabe, R. 2001, in *ASP Conf. Ser.* 249, *The Central Kiloparsec of Starbursts and AGN: The La Palma Connection*, ed. J. H. Knapen, J. E. Beckman, I. Shlosman, & T. J. Mahoney (San Francisco: ASP), 672
- Kohno, K. 2005, *AIP Conf. Proc.* 783, *The Evolution of Starbursts: The 331st Wilhelm and Else Heraeus Seminar*, ed. S. Hüttemeister, E. Manthey, D. Bomans, & K. Weis, 203
- Kohno, K., Ishizuki, S., Matsushita, S., Vila-Vilaró, B., & Kawabe, R. 2003, *PASJ*, 55, L1
- Kotilainen, J. K., Reunanen, J., Laine, S., & Ryder, S. D. 2000, *A&A*, 353, 834
- Krips, M., Eckart, A., Neri, R., Pott, J. U. , Leon, S., Combes, F., García-Burillo S., Hunt, L. K., Baker, A. J. , Tacconi, L. J., Englmaier, P., Schinnerer, E., & Boone, F. 2005, *ApJ*, 442, 479
- Krips, M., Neri, R., García-Burillo S., Combes, F., Schinnerer, E., Baker, A. J., Eckart, A., Boone, F., Hunt, L., Leon, S., & Tacconi, L. J. 2007, *A&A*, 468, L63
- Lavezzi, T. E., Dickey, J. M., Casoli, F., & Kazès, I. 1999, *AJ*, 117, 1995
- Lepp, S. & Dalgarno, A., 1996, *A&A*, 306, L21
- Lindt-Krieg, E., Eckart, A., Neri, R. , Krips, M., Pott, J.-U., García-Burillo S., Combes, F. 2008, *ApJ*, 479, 377
- Matsushita, S., Kohno, K., Vila-Vilaró, B., Tosaki, T., & Kawabe, R. 1998, *ApJ*, 495, 267
- Matsushita, S., Sakamoto, Kazushi, Kuo, Cheng-Yu, Hsieh, Pei-Ying, Dinh-V-Trung, Mao, Rui-Qing, Iono, Daisuke, Peck, Alison B., Wiedner, Martina C., Liu, Sheng-Yuan, Ohashi, Nagayoshi, & Lim, Jeremy 2004, *ApJ*, 616, L55
- McKee, C. F., Storey, J. W. V., Watson, D. W., & Green, S. 1982, *ApJ*, 259, 647
- Meier, D. S., Turner, J. L., & Hurt, R. L. 2000, *ApJ*, 531, 200
- Meijerink, R., Spaans, M., & Israel, F. P. 2007, *A&A*, 461, 793
- Ondrechen, M. P., van der Hulst, J. M., & Hummel, E. 1989, *ApJ*, 342, 39
- Petitpas, G. R., & Wilson, C. D. 2003, *ApJ*, 587, 649
- Prieto, M. A., Maciejewski, W. & Reunanen, J. 2005, *ApJ*, 130, 1472



- Quillen, A. C., Frogel, J. A., Kuchinski, L. E., & Terndrup D. M. 1995, *AJ*, 110, 156
- Rickard, J. J. 1975, *A&A*, 40, 339
- Richardson, K. J., White, G. J., Avery, L. W., Lesurf, J. C. G., & Harten, R. H. 1985, *ApJ*, 290, 637
- Rotaciuc, V., Krabbe, A., Cameron, M., Drapatz, S., Genzel, R., Sternberg, A., Storey, & J. W. V., 1991, *ApJ*, 370, 23
- Rubin, V. C., Thonnard, N., & Ford, W. K., Jr. 1980, *ApJ*, 238, 471
- Rubin, V. C., Ford, W. K., Jr., Thonnard, N., & Burstein, D. 1982, *ApJ*, 261, 439
- Sakamoto, S., Hayashi, M., Hasegawa, T., Handa, T., & Oka, T. 1994, *ApJ*, 425, 641
- Sakamoto, K., Okumura, S. K., Ishizuki, S., & Scoville, N. Z. 1999, *ApJ*, 525, 691
- Schinnerer, E., Eckart, A. & Tacconi, L. J. 2000, *ApJ*, 533, 826
- Schinnerer, E., Eckart, A., Tacconi, L. J., Genzel, R., & Downes, D. 2000, *ApJ*, 533, 850
- Scoville, N. Z., Yun, M. S., Clemens, D. P., Sanders, D. B., & Waller, W. H. 1987, *ApJS*, 63, 821
- Scoville, N. Z., Yun, M. S., Armus, L., & Ford, H. 1998, *ApJ*, 493, L63
- Seta, M., Hasegawa, Tetsuo, Dame, T. M., Sakamoto, Seiichi, Oka, Tomoharu, Handa, Toshihiro, Hayashi, Masahiko, Morino, Jun-Ichi, Sorai, Kazuo, & Usuda, Kumiko S. 1998, *ApJ*, 505, 286
- Sofue, Y., Tutui, Y., Honma, M., Tomita, A., Takamiya, T., Koda, J., & Takeda, Y. 1999, *ApJ*, 523, 136
- Solomon, P. M., Rivilo, A. R., Barrett, J., & Yahil, A. 1987, *ApJ*, 319, 730
- Storchi-Bergmann, T., Baldwin, J. A., & Wilson, A. S. 1993, *ApJ*, 410, L11
- Storchi-Bergmann, T., Wilson, A. S., & Baldwin, J. A. 1996, *ApJ*, 460, 252
- Tacconi, L. J., Genzel, R., Blietz, M., Cameron, M., Harris, A. I., & Madden, S., 1994, *ApJ*, 426, 77
- Terashima, Y., Iyomoto, N., Ho, L. C., & Ptak, A. F. 2002, *ApJS*, 139, 1

- Tully 1988, *Nearby Galaxies Catalog* (Cambridge: Cambridge University Press)
- Turner, J. L., Hurt, R. L., & Hudson, D. Y. 1993, *ApJ*, 413, L19
- Usero, A., García-Burillo, S. Fuente, A. Martín-Pintado, J., & Rodríguez-Fernández, N. J., 2004, *A&A*, 419, 897
- van Dishoeck, E. F., Jansen, D. J., & Phillips, T. G. 1993, *A&A*, 279, 541
- Wada, K., & Norman, C. A. 2002, *ApJ*, 566, L21
- Weiss, A., Neininger, N., Hüttemeister, S., & Klein, U. 2001, *A&A*, 365, 571

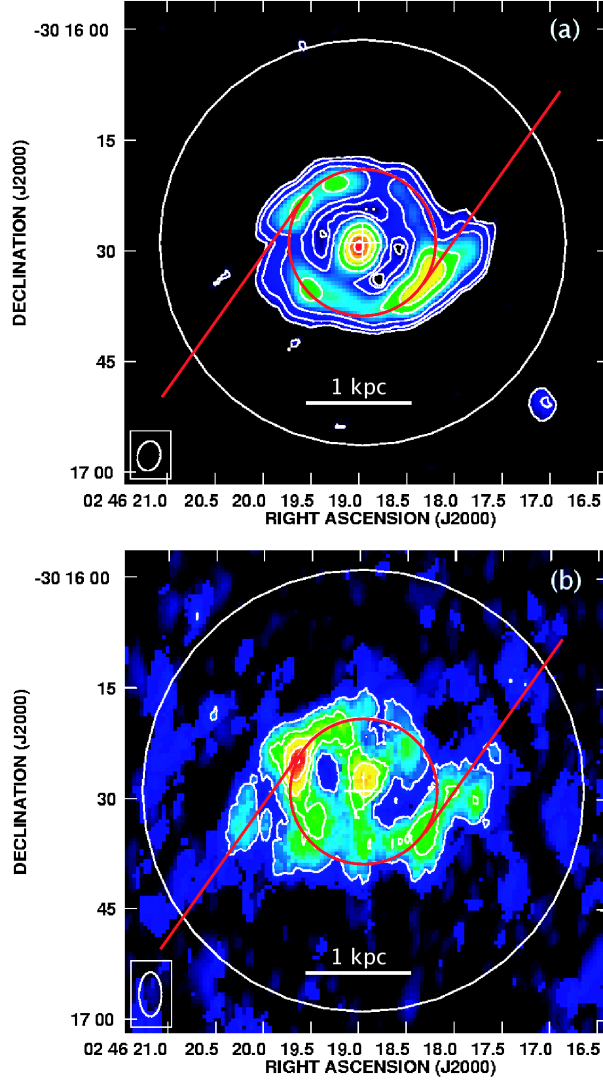


Fig. 1.— (a)  $^{12}\text{CO}(J=2-1)$  integrated intensity (moment 0) map of the central region of NGC 1097. The contour levels are  $(2.5, 5, 10, 20, 30, 40, \text{ and } 50) \times 3.7 \text{ Jy beam}^{-1} \text{ km s}^{-1}$ , where  $1\sigma$  is  $3.7 \text{ Jy beam}^{-1} \text{ km s}^{-1}$ . The synthesized beam is  $3''.1 \times 4''.1$  with a P.A. of  $168^\circ$ , which is shown in the bottom-left corner of the map. The large white circle is the primary beam size ( $52''$ ) of the SMA. (b)  $^{12}\text{CO}(J=1-0)$  integrated intensity map. The contour levels are  $(2.5, 5, 7, 9, \text{ and } 11) \times 3.9 \text{ Jy beam}^{-1} \text{ km s}^{-1}$ , where  $1\sigma$  is  $3.9 \text{ Jy beam}^{-1} \text{ km s}^{-1}$ . The synthesized beam is  $6''.0 \times 3''.0$  with a P.A. of  $0^\circ$ , which is shown in the bottom-left corner. The large white circle is the primary beam size ( $63''$ ) of the NMA. In both images, the central crosses mark the peak of the 6 cm continuum (Hummel et al. 1987), the small red circles at a radius of  $10''$  mark the radius of the molecular ring, and the two red lines mark the positions of the dust lanes.

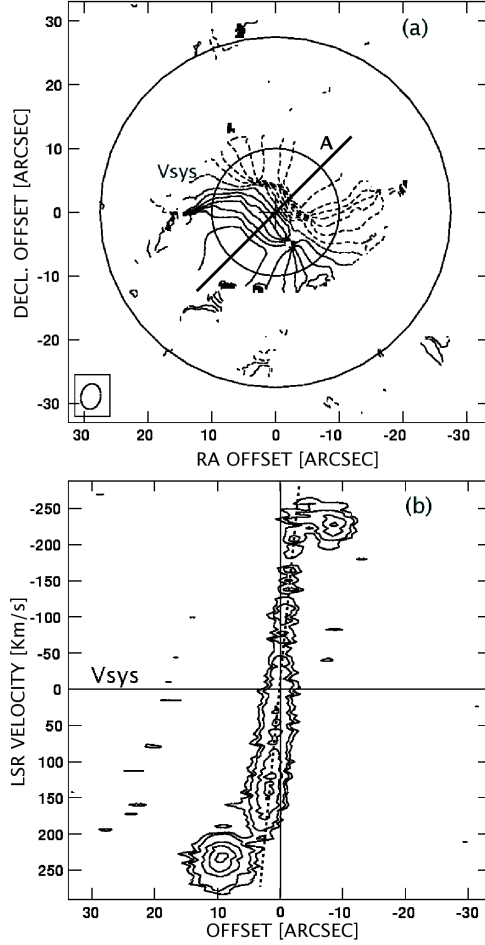


Fig. 2.— (a) Intensity-weighted mean velocity (moment 1) map of  $^{12}\text{CO}(J=2-1)$ . Large and small circles are marked as the primary beam size of the SMA (52'') and the size of starburst ring (radius of 10''), respectively. The systemic velocity (1254 km s $^{-1}$ ; Kohno et al. 2003) is marked. The contour interval is 15 km s $^{-1}$ . Dotted and solid curves are the blueshifted and redshifted velocities, respectively. The solid line labeled as “A” represents the direction of the major axis (P.A. is 135°) of NGC 1097 (Hummel et al. 1987). The nuclear gas is rotating with the molecular ring in the same sense, while it is rotating faster than the ring. (b) Position-velocity diagram of the  $^{12}\text{CO}(J=2-1)$  emission cut along the major axis (represented as “A” in the above figure). Contour levels are 3, 5, 10, 15, and 20 $\sigma$ , where 1 $\sigma$  = 75 mJy beam $^{-1}$ . The zero velocity corresponds to the systemic velocity of 1254 km s $^{-1}$  marked as horizontal solid lines. The offset of 0'' corresponds to the galactic center, and the LSR velocity of 0 km s $^{-1}$  corresponds to the systemic velocity. The fitted velocity gradient (1.31 km s $^{-1}$ ) of the nuclear component is marked as a dash line. Note that the inclination of the galactic disk is not corrected.

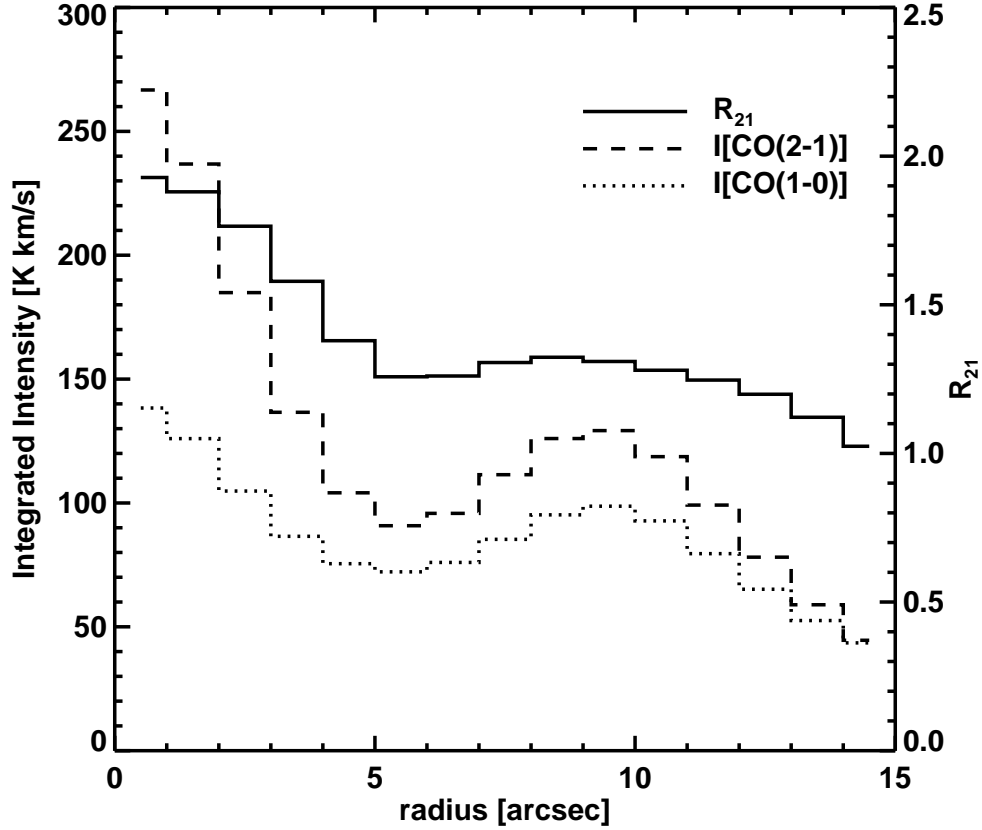


Fig. 3.— Azimuthally averaged radial intensity distributions of the  $^{12}\text{CO}(J = 2 - 1)$  (dashed line) and  $^{12}\text{CO}(J = 1 - 0)$  (dotted line) lines in brightness temperature scale. The temperature scale is shown in the left-hand side of the vertical axis. Azimuthally averaged radial distribution of  $R_{21}$  is marked as a solid line. The ratio scale is shown in the right-hand side of the vertical axis.

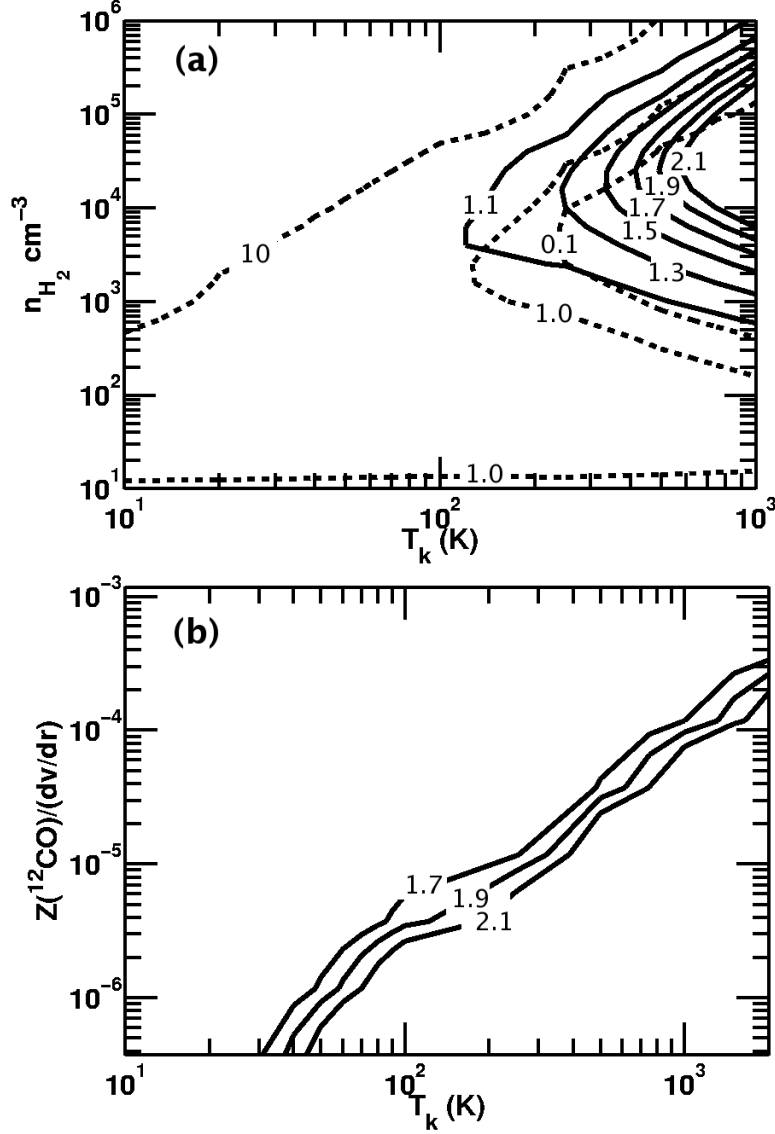


Fig. 4.— (a)  $R_{21}$  is plotted as a function of kinetic temperature  $T_k$  and H<sub>2</sub> number density  $n_{H_2}$  at a standard  $Z(^{12}\text{CO})/(dv/dr)$  of  $5.0 \times 10^{-5} (\text{km s}^{-1} \text{ pc}^{-1})^{-1}$ . Solid lines are the  $R_{21}$  of the nuclear component ( $1.9 \pm 0.2$ ) and the molecular ring ( $1.3 \pm 0.2$ ). Opacity for  $^{12}\text{CO}(J = 1 - 0)$  is marked as dashed lines. (b)  $R_{21}$  of the nuclear component is plotted as a function of  $T_k$  and  $Z(^{12}\text{CO})/(dv/dr)$ . Solid lines are the observed  $R_{21}$  of the nuclear component with  $n_{H_2}$  fixed at a value of  $1.0 \times 10^4 \text{ cm}^{-3}$ .